Electronic Supplementary Information

$\{Dy(\alpha\text{-fur})_3\}_n$: from double relaxation Single-Ion Magnet behavior to 3D ordering

E.Bartolomé,[a] J. Bartolomé, [b] S. Melnic,[c] D. Prodius,[c] S. Shova,[d] A. Arauzo,[e] J. Luzón,[b,f] F. Luis,[b] and C. Turta[c]

[a] *Escola Universitària Salesiana de Sarrià, Passeig Sant Joan Bosco 74, 08017-Barcelona, Spain. Fax: +34 932806642; Tel: +34-932805244; E-mail: ebartolome@euss.es*

[b] *Instituto de Ciencia de Materiales de Aragón, CSIC-Universidad de Zaragoza, Pedro Cerbuna 12, 50009 Zaragoza, Spain.*

[c] *Institute of Chemistry, Academy of Sciences of Moldova, Academiei 3, MD-2028,Chisinau, Moldova*

[d] *Institute of Macromolecular Chemistry "Petru Poni" Iasi, Aleea Grigore Ghica Voda, nr. 41A, 700487 Iasi, Romania*

[e] *Servicio de Medidas Físicas. Universidad de Zaragoza, Pedro Cerbuna 12, 50009 Zaragoza, Spain.*

[f] *Centro Universitario de la Defensa. Academia General Militar, Zaragoza, Spain.*

SI. Identification of magnetic relaxation processes at H=0 and H=4 kOe

The real χ' and imaginary χ'' components of the ac susceptibility as a function of the temperature T and frequency $f=\omega/2\pi$ were measured at H=0 and 4 kOe, for the pure (x=0) and diluted sample (x=0.9). Different magnetic relaxation processes could be identified from the χ', χ'' data as the (H, T, f) conditions were varied. In this section, the assignation of , χ'' peaks to the different relaxation processes is shown.

- At H=0, two different measurement runs were performed:

  Raw data Run 1: χ', $\chi''(f)$, with $0.01<f<10^4$ (Hz), at different constant temperatures (1.9 - 6.4 K)

  Raw data Run 2: χ', $\chi''(T)$, with $2<T<10$ (K), at different constant frequencies (10 - 9333 Hz)

- At H=4 kOe only run 1 was carried out.

It was realized that, in some cases, a broad $\chi''(f)$ peak masked several different processes, which could not be separated. However, by representing the same raw data as $\chi''(T)$, at different constant frequencies, the different processes became distinguishable. In the next Figs. S1-S4, we present: the χ', $\chi''(f$, different constant T) plots and corresponding transformed χ', $\chi''(T$, different constant f) plots obtained from run 1, the χ', χ'' (T, different constant f) measured in run 2 and the relaxation time as a function of the inverse temperature, $\tau(1/T)$, deduced from the χ'' peaks in both representations assuming that at the maximum $\tau\omega=1$ ($\omega=2\pi f$). In the $\tau(1/T)$ plot the points coming from the different runs and representations have been distinguished with different symbols. Moreover, to facilitate the identification of the different processes, the positions of the peaks in the $\chi''(T, f)$ curves have been marked with the same symbols used in the $\tau(1/T)$ plot. As deduced from X-ray experiments, $\{Dy(\alpha\text{-fur})_3\}_n$ complex contains two non-equivalent Dy sites, A and B, which relax differently. In Figs. S1-S4, points coming from the relaxation of Dy(A) and D(B) sites have been marked with reddish and bluish colors, respectively.

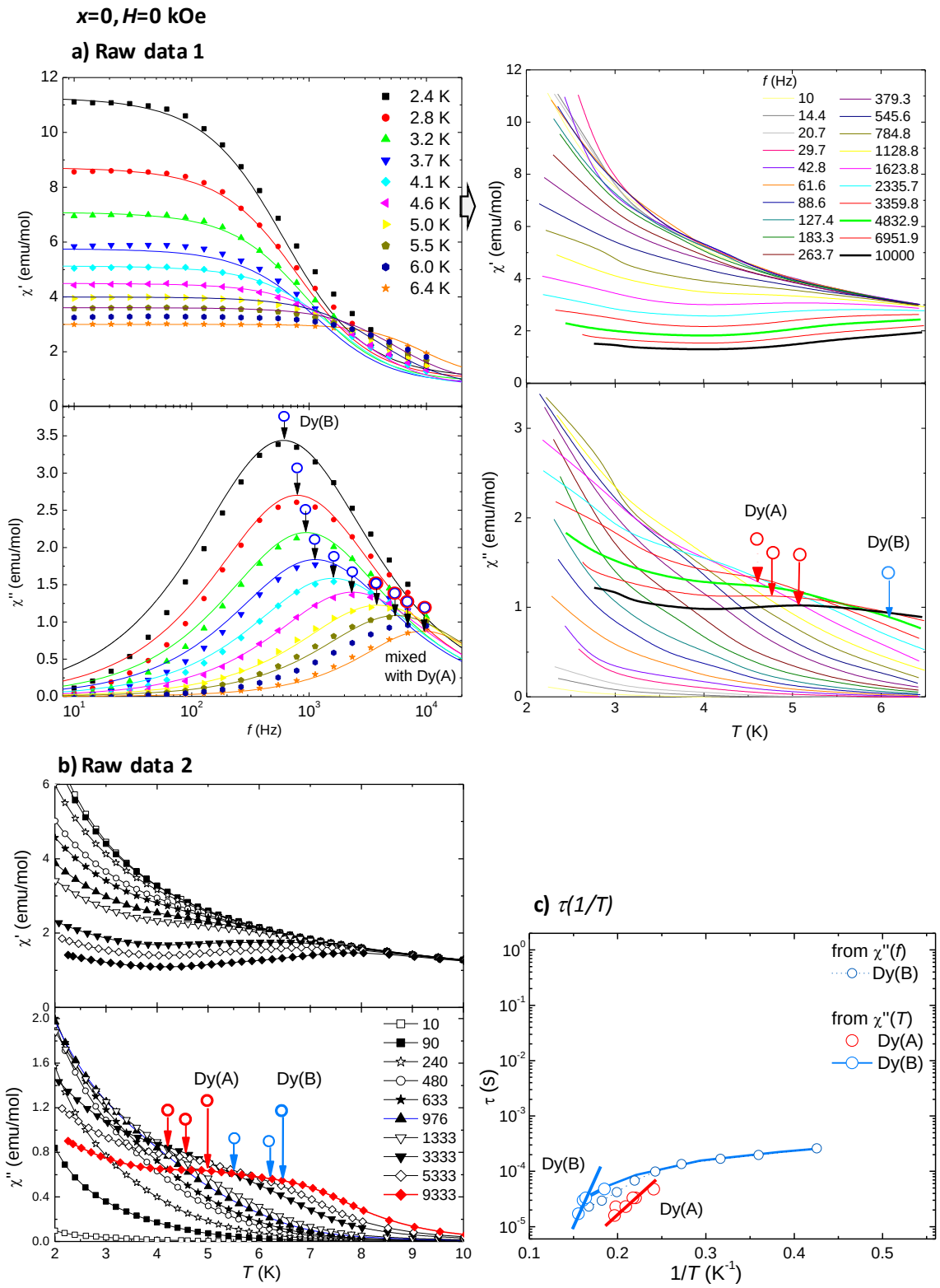

Fig. S1. Relaxation data for undiluted sample *x*=0, at *H*=0: *a) Raw data 1: Left:* χ', χ''(*f*, at different *T*) plots: the χ''(*f*) peak at low temperatures corresponds to the relaxation of the Dy(B) type. At higher temperatures the broad peak probably contains a contribution of the Dy(A) type; *Right:* χ', χ''(*T*, at different *f*) plots deduced from the former data; *b) Raw data 2:* χ', χ'' (*T*, at different *f*) plot obtained from a different measurement run covering a larger, 2<*T*<10 K range, where the TAQT relaxation of the two species can be appreciated; c) Relaxation time *vs.* 1/*T* determined from the peaks observed in the χ''(*T*) and χ''(*f*) representations.

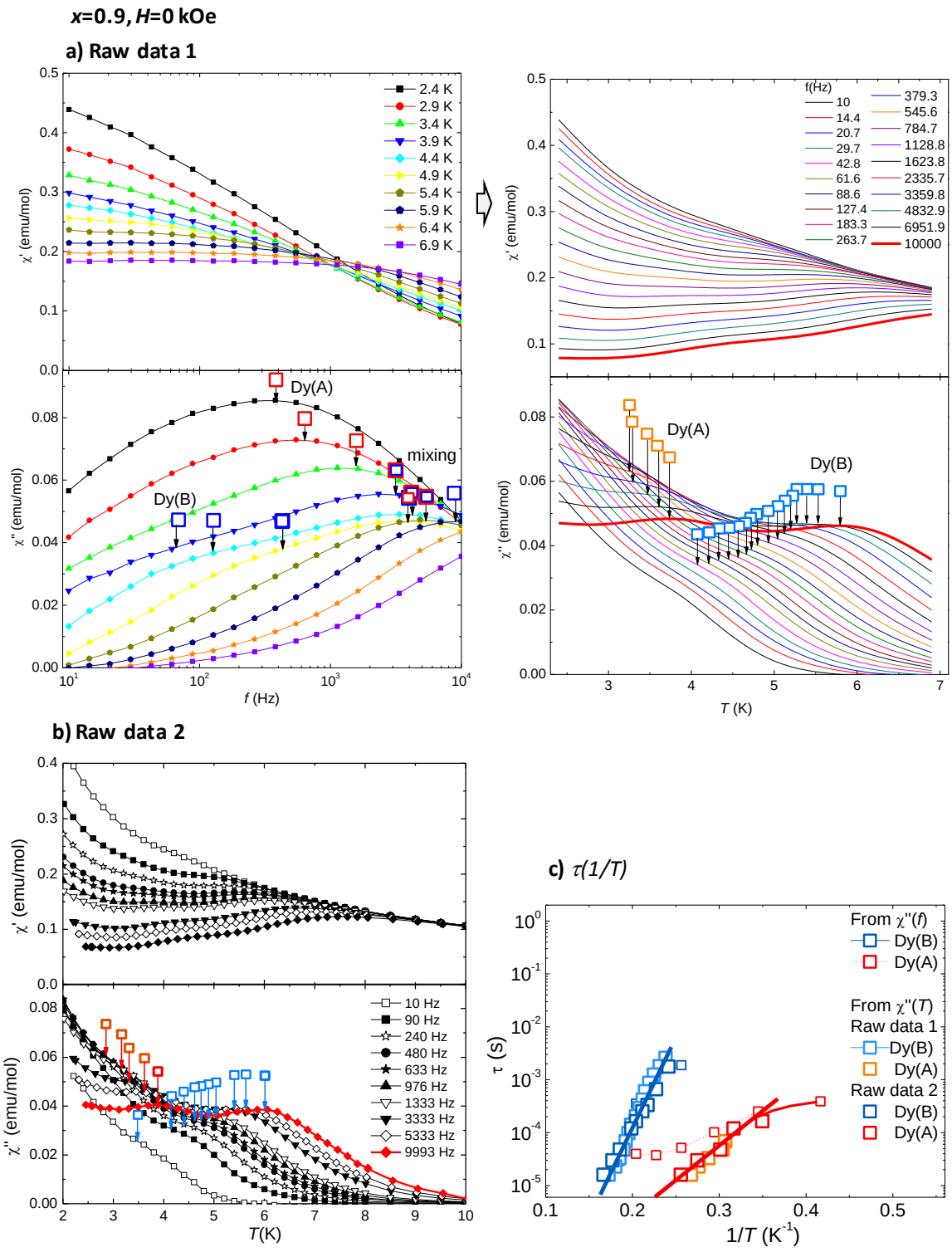

Fig. S2. Relaxation data for diluted sample *x*=0.9, at *H*=0: *a) Raw data 1: Left:* χ', χ''(*f*, at different *T*) plots, where the signatures of relaxation of the Dy(A) and Dy(B) types have been signaled. At high temperatures the broad peak contains the contribution from the two species; *Right:* χ', χ''(*T*, at different *f*) plots deduced from the former data, where the position of the relaxation peaks of the two Dy types can be better appreciated; *b) Raw data 2:* χ', χ'' (*T*, at different *f*) plot obtained from a second measurement run covering a larger, 2<*T*<10 K range, where the TAQT relaxation of the two species is clearly distinguished; c) Relaxation time *vs.* 1/*T* determined from the χ''(*T*) and χ'(*f*) representations. Note: the $\tau(1/T)$ data obtained from the χ''(*f*) peaks containing mixed contributions (linked by a red dashed line) fall in between the TAQT linear ln $\tau(1/T)$ dependences of Dy(A) and Dy(B).

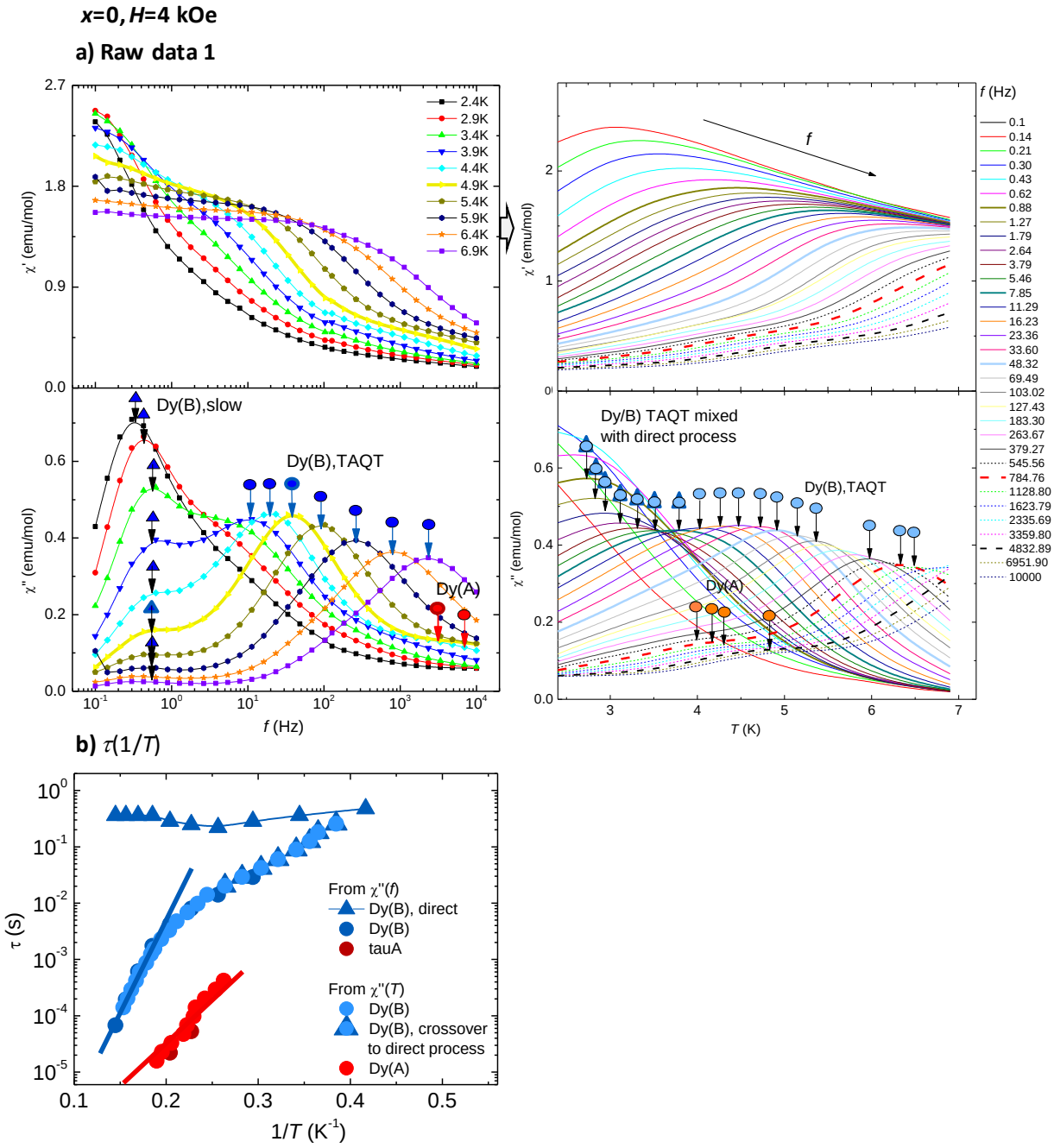

Fig. S3. Relaxation data for undiluted sample *x*=0, at *H*=4 kOe: ***a)*** *Raw data 1: Left:* χ', χ''(*f*, at different *T*) plots, showing the the TAQT relaxation of Dy(A) and Dy(B) types at high frequencies, and an additional peak at very low frequencies attributed to relaxation of Dy(B) by a direct process. As the temperature is decreased, the peak corresponding to Dy(B) TAQT mechanism decreases its intensity, whereas the direct process peak increases. Note there is an intermediate region where both mechanisms occur simultaneously. *Right:* χ', χ''(*T*, at different *f*) plots deduced from the former data, where the position of the TAQT relaxation peaks of the two Dy species are signaled. As the frequency is decreased, the Dy(B) peak contains an increasing contribution from the slow, direct process; c) Relaxation time *vs.* 1/*T* determined from the χ''(*T*) and χ'(*f*) representations. Note there is a region of temperatures where Dy(B) can relax either via TAQT or direct process; as the temperature is decreased, a crossover towards a direct process occurs (blue circle/triangles symbols).

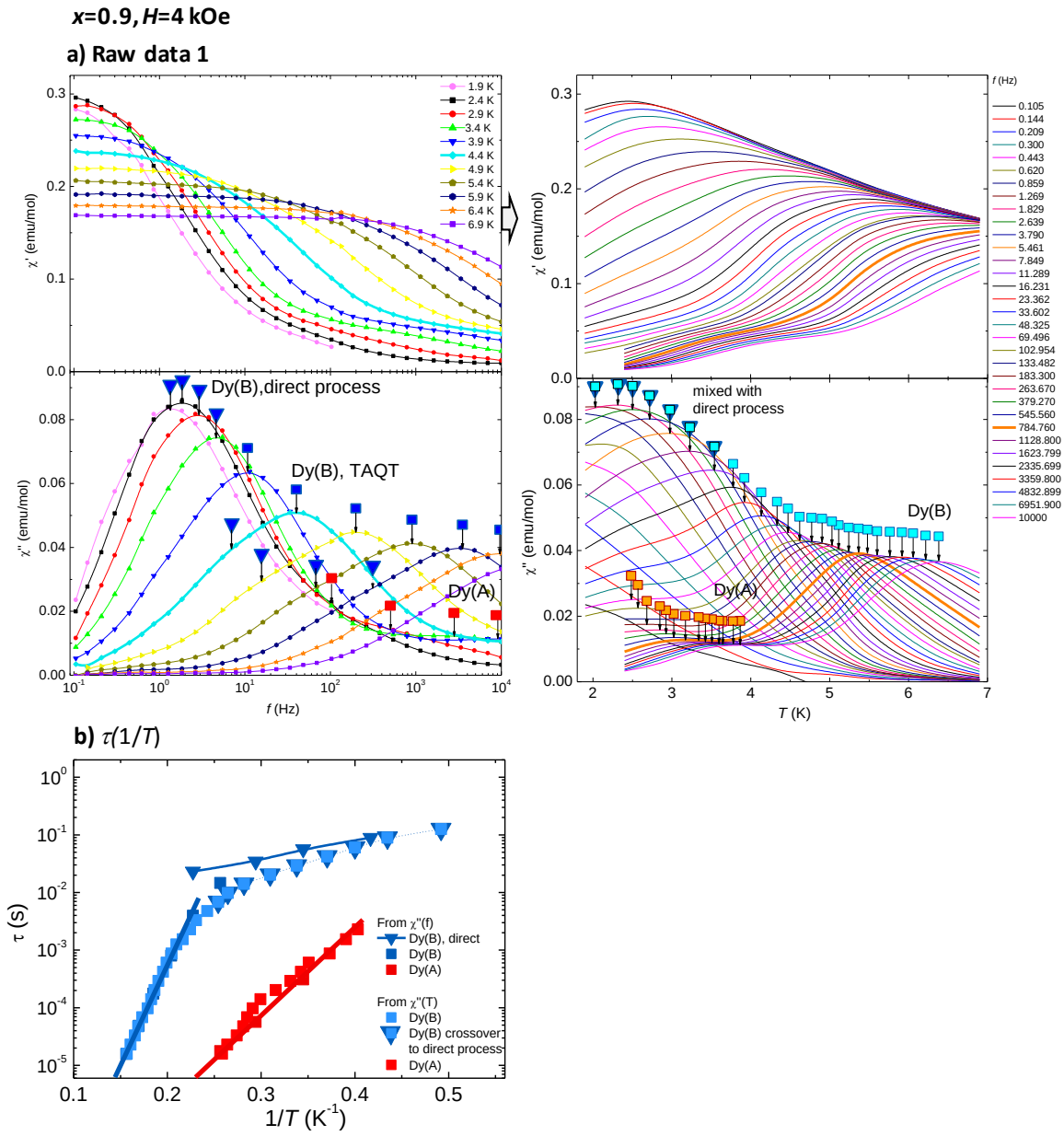

Fig. S4. Relaxation data for undiluted sample *x*=0.9, at *H*=4kOe: ***a****) Raw data 1: Left:* χ', χ''(*f*, at different *T*) plots, showing the TAQT relaxation of Dy(A) and Dy(B) types at high frequencies, and a peak attributed to a direct process of Dy(B) at very low *f*. As *T* is decreased, the peak corresponding to Dy(B) TAQT mechanism decreases its intensity, whereas the direct process peak increases. *Right:* χ', χ''(*T*, at different *f*) plots deduced from the former data, where the position of the TAQT relaxation peaks of the two Dy species are signaled. As the frequency is decreased, the Dy(B) peak contains an increasing contribution of the direct process mixed with the TAQT process; c) Relaxation time *vs.* 1/*T* determined from the χ''(*T*) and χ'(*f*) representations. For the Dy(B) type, note the transition from the TAQT linear dependence to the direct process curve (blue square/triangle symbols).

Table S1. Characteristic relaxation times, τ_0, activation energies, *U*, of the TAQT relaxation processes and Quantum Tunneling characteristics τ_T corresponding to the Dy(A) and Dy(B) types, for the pure (*x*=0) and diluted (*x*=0.9) samples, at *H*=0 and *H*=4 kOe.

		Dy(A)		Dy(B)	
		x=0	*x*=0.9	*x*=0	*x*=0.9
H=0 kOe	U/k_B (K)	29(3)	30(2)	80(3)	77(3)
	τ_0 (s)	$5(3)\times10^{-8}$	$7(3)\times10^{-9}$	$6(4)\times10^{-11}$	$3(1)\times10^{-11}$
	τ_T (s)	-	$4(1)\times10^{-4}$	$3(2)\times10^{-4}$	-
H=4 kOe	U/k_B (K)	38(5)	32.4(5)	79(3)	80.5(6)
	τ_0 (s)	$2(1)\times10^{-8}$	$4.5(5)\times10^{-9}$	$7(1)\times10^{-10}$	$5.7(2)\times10^{-11}$
	τ_T (s)	-	-	$4(1)\times10^{-1}$	$1(1)\times10^{-1}$

SII. Identification of magnetic relaxation processes as a function of the field

The real χ' and imaginary χ'' components of the ac susceptibility as a function of frequency $f=\omega/2\pi$ were measured at T=2.4 K at different applied fields between 0 – 4 kOe, for the pure (x=0) and diluted sample x=0.9 (Fig. S5). Figure S6 summarizes the field-dependence of the relaxation time, $\tau(H)$, and the intensity of the peaks, $\chi''_{max}(H)$, for the different processes observed.

SIII. Simulation of powder a.c. susceptibility field dependence in the quantum tunneling regime

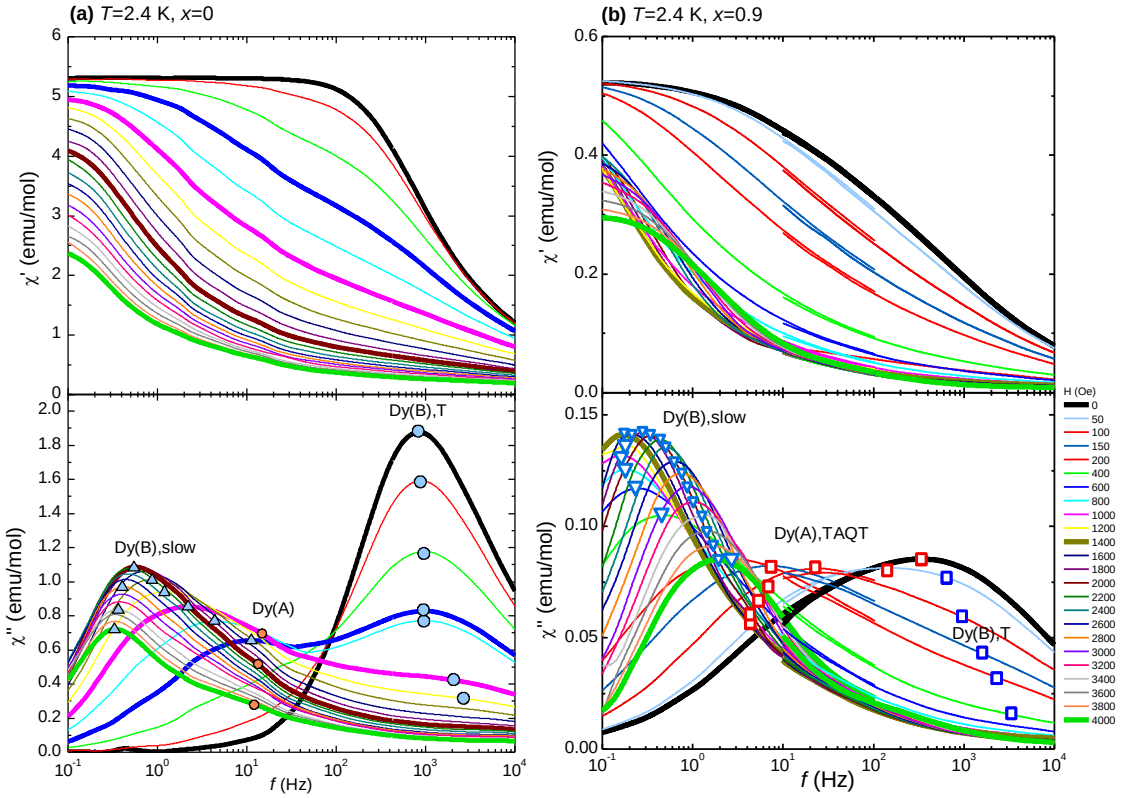

Fig. S5. χ', χ''(f) at different applied fields at T=2.4 K, for pure (a), and diluted sample x=0.9 (b).

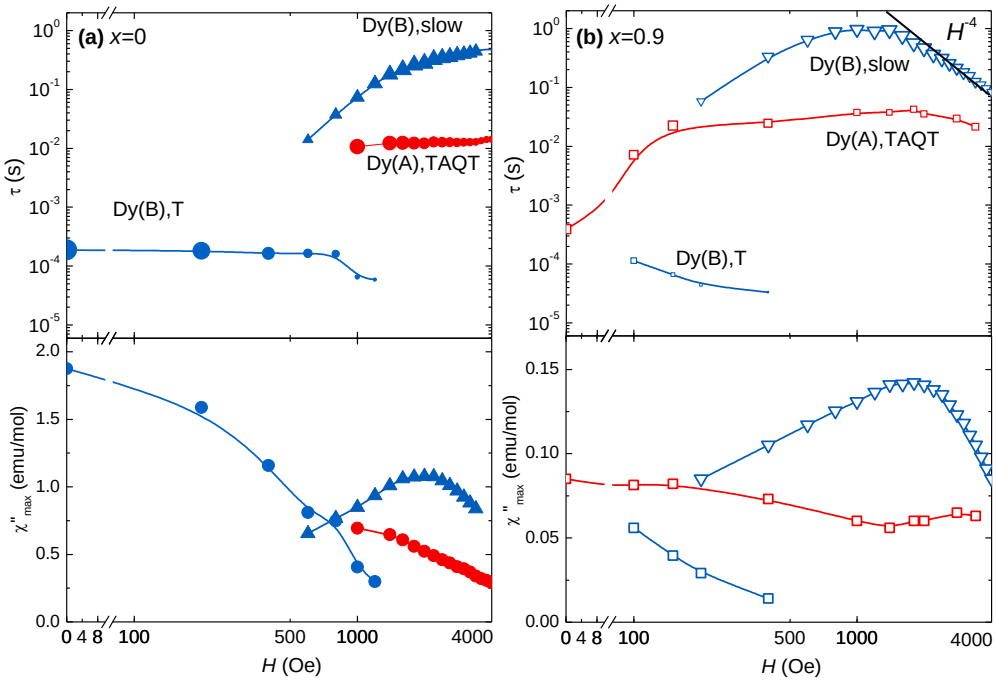

Fig. S6. Field-dependence of the relaxation time, $\tau(H)$, and intensity of the peaks, $\chi''_{max}(H)$, for the different

The inversion of the magnetic moment direction in an uniaxial anisotropic hindering barrier may occur at very low temperature and zero field, through resonant tunneling between the ground state degenerate levels, or at $H \neq 0$, when there is level crossing of the Zeeman split electronic states. In the case they consist of Kramers doublets resonant tunneling is forbidden, unless dipole-dipole and exchange interaction and non-local symmetry perturbs the diagonal Hamiltonian, allowing the mixing of the two states [1].

The ligand field interaction splits the $^6H_{15/2}$ Dy ground multiplet into Kramers doublets. For a Dy ion, with high uniaxial single ion anisotropy, the ground state doublet anisotropy is described by its $\hat{g}^*$ tensor components $g_x^* = g_y^* << g_z^*$, and the bias field is caused essentially by dipolar interactions. Hyperfine effects could play also a role since two isotopes support a nuclear moment that could contribute to the bias field through the hyperfine interaction; namely, ^{161}Dy and ^{163}Dy isotopes, with a natural abundance of 18.8 and 24.9 %, respectively, both have a I=5/2 nuclear spin. It could play a role at very low temperature, depending on the hyperfine interaction constant value. In $\{Dy(\alpha\text{-fur})_3\}_n$, no hyperfine effects have been observed down to 60 mK, so this contribution is considered as negligible.

According to the Proko'fev and Stamp [2, 3] approximation, at H=0, the average bias dipolar field is zero, and consequently, no tunneling would be possible. However, there are spin fluctuations that give rise to a broadening in the probability of non-zero dipolar fields $P(\sigma_{dip,z})$, at any given time. The transverse component of this non-zero field $\sigma_{\xi dip,xy}$, promotes tunneling. However, the tunneling energy window $\Delta_T = g_{xy}^* \mu_B H_{dip,xy}$ is very small with respect to the dipolar bias energy $\xi_{dip} = g_z^* \mu_B H_{dip,z}$, so the transition tunneling probability of a probe spin is very small. It is assumed that the subsequent rearrangement of the spins after reversal by tunneling of that probe spin modifies the spin arrangement and allows to invert some formerly improbable moments. Given sufficient time, the whole spin array may have the possibility to tunnel, and the QT process may become macroscopically observable.

The characteristic time of the tunneling process can be related to the distribution of energy bias of dipolar energy, $P(\xi_{dip}) = g_z^* \mu_B P(\sigma_{dip,z})$, and the tunneling energy Δ_T [2]:

$$\tau(H,\theta) = \frac{\hbar}{\Delta_T^2(H,\theta) P(\xi_{dip})}, \qquad [1]$$

If $P(\xi_{dip})$ is assumed to be a Gaussian function,

$$P(\xi_{dip}) = \frac{1}{\sqrt{2\pi} g_z^* \mu_B \sigma_{dip,z}} exp\left(-\frac{\xi_{dip}^2}{2 g_z^{*2} \mu_B^2 \sigma_{dip,z}^2} \right), \qquad [2]$$

that for H=0 and θ=0, then only the spins with a dipolar energy $\xi_{dip} \approx 0$ fall within the condition for tunneling, $-\Delta_T / 2 < \xi_{dip} < \Delta_T / 2$, and the tunneling time constant is obtained:

$$\tau = \frac{\hbar}{\Delta_T^2 P(\xi_{dip} = 0)} . \qquad [3]$$

If an external field H is applied at an angle θ with the anisotropy axis z, only those spins with $\xi_{dip} = \pm \xi_{Zeeman}$, that is, with a dipolar energy that is compensated by the Zeeman term so that the total energy is within the tunneling window, will undergo spin reversion by QT. The bias energy is:

$$\xi_{dip} = \pm g_z^* \mu_B H cos\theta , \qquad [4]$$

and the tunneling splitting:

$$\Delta_T(H,\theta) = g_{xy}^* \mu_B \left(\sigma_{dip,xy} + H sin\theta \right) . \qquad [5]$$

Substituting in Eq. [1], one obtains the dependence of the tunneling time constant:

$$\tau(H,\theta) = \frac{\hbar \sqrt{2\pi} g_z^* \sigma_{dip,z}}{\mu_B g_{xy}^{*\,2} \mu_B \left(\sigma_{dip,xy} + H sin\theta \right)^2} exp\left(\frac{H^2 cos^2\theta}{2\sigma_{dip,z}^2} \right). \qquad [6]$$

The real and imaginary components of the a.c. susceptibility are obtained by substituting $\tau(H,\theta)$ in the Kramers-Kronig equations for a fixed temperature and excitation frequency:

$$\chi'(\omega,T,H,\theta)=\frac{[\chi_T(T,H,\theta)-\chi_S]}{1+\omega^2\tau(H,\theta)^2}+\chi_S\,, \qquad [7a]$$

$$\chi''(\omega,T,H,\theta)=\frac{\chi_T(T,H,\theta)}{1+\omega^2\tau(H,\theta)^2}\,, \qquad [7b]$$

where:

$$\chi_T(T,H,\theta)\approx(2g_{xy}^{*\,2}\sin^2\theta+g_z^{*2}\cos^2\theta)\mu_B^2/3k_BT\,. \qquad [8]$$

The final step consists in calculating numerically the angular averaging over angle θ:

$$\chi(\omega,T,H)=\frac{\int_0^{\pi}\chi(T,H,\theta)\sin\theta d\theta}{\int_0^{\pi}\sin\theta d\theta}\,. \qquad [9]$$

In the $\{Dy(\alpha\text{-fur})_3\}_n$ case, for the Dy(B) center, the experimental parameters used have been $\tau_T\approx3\text{x}10^{-4}$ s, $\xi_{dip}/k_B\approx T_N=0.66$ K and the width of the bias field $\sigma_{dip,z}=500$ Oe. The value of $g_z^*=19.5$ has been fixed, after the *ab initio* calculations. The $\chi''(f=2\pi\omega)$ curves have a single maximum at each field, that decreases strongly in height and broadens in ln*f*. The average tunneling time, as deduced from the condition $\omega\tau=1$, thus, are evaluated at each field. In the present case, for increasing field it decreases for small fields, shows a minimum at a field 700<H<1000 Oe, and increases for larger fields. The slope of the decrease depends strongly on the ratio $\sigma_{\xi dip,xy}/\sigma_{\xi dip,z}$, as depicted in Fig. S7.

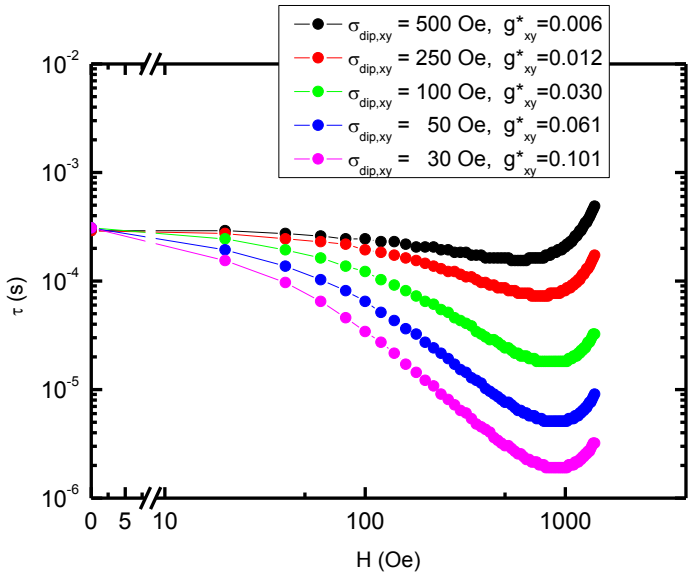

Fig. S7. $\tau_T(H)$ calculated after the simulations of $\chi''(f, H)$, for varying $\sigma_{dip,\,xy}$ and g_{xy}* values.

The calculation of the $\chi''(f, H)$ curves for g_{xy}*=0.0061, g_z*=19.5, and bias fields values of $\sigma_{dip,xy}=\sigma_{dip,z}=500$ Oe and $\sigma_{dip,xy}=\sigma_{dip,z}=50$ Oe (Fig. S8) reproduce qualitatively the experimental field dependence of the Dy(B) QT peak for the *x*=0 and *x*=0.9 cases respectively (Fig.S5a,b), at least for low enough fields. The stronger shift of the QT $\chi''(f)$ peak with the field observed for the *x*=0.9 compound is thus explained by the simulations in terms of a decrease of the bias field, proportional to the magnetic dilution. The simulated $\chi''(f, H)$ peak value is larger than

the experiment since it has been assumed in the simulation that all spins belong to the same type (Dy(B)), while in the experiment the Dy atoms are distributed in Dy(A) and Dy(B) types.

The comparison between the experimental and low field simulations of $\chi''(f)$ for a powder sample let us prove that the tunneling relaxation rate may decrease or remain close to constant with the field, depending on the actual values of $\sigma_{\mathrm{dip,xy}}$ and g^{*}_{xy}.

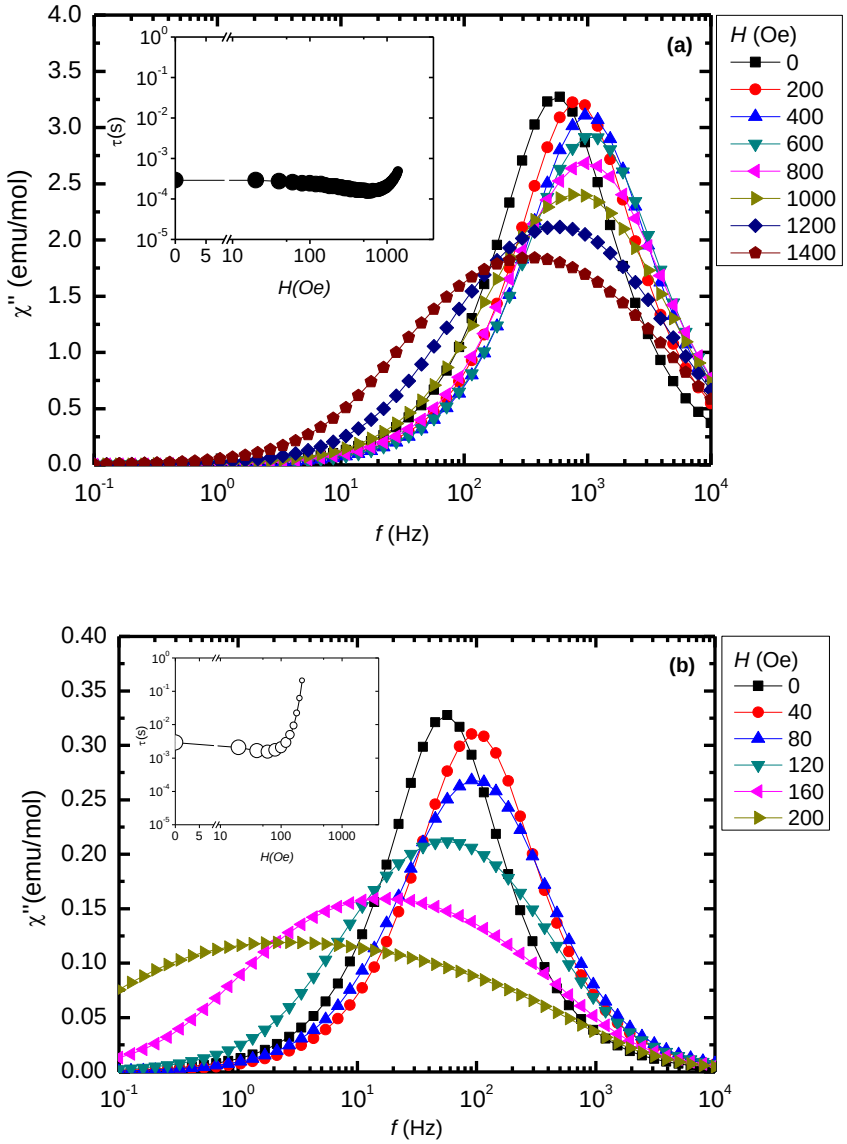

Fig. S8. Simulations of $\chi''(f, H)$ curves for the values g_{xy}*=0.0061, g_z*=19.5, with (a) $\sigma_{\mathrm{dip,xy}}=\sigma_{\mathrm{dip,z}}$=500 Oe and (b) $\sigma_{\mathrm{dip,xy}}=\sigma_{\mathrm{dip,z}}$=50 Oe, mimicking the x=0 and x=0.9 experimental cases (Figs. S5a,b), respectively.

References

[1] D. Loss, D. P. DiVincenzo, and G. Grinstein, *Phys. Rev. Lett.*, 1992, **69**, 3232.
[2] N. V. Prokof'ev and P.C.E. Stamp, *Phys. Rev. Lett.*, 1998, **80**, 5794.
[3] W. Wernsdoerfer, T. Ohm, C. Sangregorio, R. Sessoli, D. Mailly, C. Paulsen, *Phys. Rev. Lett.*, 1999, **82**, 3903.